



Nonlinear Stability and Transition in 3-D Boundary Layers

WILLIAM S. SARIC, RUBEN B. CARRILLO, JR. and MARK S. REIBERT
Arizona State University, Mechanical and Aerospace Engineering, Tempe, AZ 85287-6106, U.S.A.

(Received: 26 May 1998)

Abstract. The important recent progress in three-dimensional boundary-layer transition research is reviewed with emphasis on the crossflow instability that leads to transition on swept wings with a favorable pressure gradient. Following a brief overview of swept-wing instability mechanisms and the crossflow problem, a summary of the important findings of the 1990s is given. The discussion is presented from the experimental viewpoint, and where appropriate, relevant comparisons with CFD are drawn. The recent research conducted with distributed roughness is described in more detail in order to underscore the latest developments concerning nonlinear effects and transition control.

Sommario. I recenti importanti sviluppi sullo studio della transizione in uno strato limite tridimensionale sono esaminati con particolare attenzione alla instabilità trasversale che conduce alla transizione su ali a freccia con gradiente di pressione favorevole. Dopo una breve descrizione dei meccanismi di instabilità sulle ali a freccia viene dato un riassunto degli importanti progressi ottenuti negli anni '90. La discussione è presentata dal punto di vista sperimentale e, ove appropriato, sono riportati confronti con la simulazione numerica. La recente ricerca, condotta con rugosità distribuita, è descritta con maggiore dettaglio allo scopo di presentare gli ultimi sviluppi concernenti gli effetti non lineari ed il controllo della transizione.

Key words: Stability, Nonlinear waves, Transition, Boundary layers, Fluid mechanics.

1. Introduction

Transition to turbulence in swept-wing flows has resisted correlation with linear theory because of its sensitivity to freestream conditions and 3-D roughness and because one of the principal instability modes quickly becomes nonlinear. In the face of such a formidable problem, two rather long-term fundamental efforts have been underway at DLR Göttingen and Arizona State University that address swept-wing transition. These efforts have been recently reviewed by Bippes [10], and Reibert and Saric [54]. Thus, the present work is a continuation of a series of studies on swept-wing boundary layers which have led to a better understanding of the transition process. In particular, we have taken advantage of the sensitivity to 3-D roughness and the modal nature of the instability in order to propose a particular control strategy.

Complementing the two afore-mentioned reviews, general reviews of the swept-wing transition problem are found in Arnal [5] and Kachanov [31]. Other recent reviews include Reshotko [56], Crouch [17], and Herbert [29, 30]. The failure of linear theory is discussed in Reed *et al.* [50]. The historical work is found in Reed and Saric [49].

The basic idea is that the combination of sweep and chordwise pressure gradient within the boundary layer creates a velocity component perpendicular to the inviscid streamline. This crossflow profile is inflectional and exhibits both traveling and stationary unstable waves called crossflow vortices that are (approximately) aligned along the inviscid streamlines. Under conditions of low freestream turbulence levels, the dominant crossflow wave is stationary [18] while moderate to high turbulence levels initiate dominant traveling waves [10, 20]. The mechanism is

relatively insensitive to sound and 2-D surface roughness [47] but very sensitive to 3-D roughness near the attachment line.

We concentrate our work on low-turbulence freestream flows and stationary crossflow waves. Although, the v' and w' components of the disturbances are very small, by convecting streamwise momentum in the wall-normal direction, they produce $O(1)$ changes in u' . Thus the mean flow is highly distorted with localized inflection points. Transition is then triggered by a high-frequency secondary instability of the distorted mean profile [33, 37].

The study of three-dimensional boundary layers is motivated by the need to understand the fundamental instability mechanisms that cause transition in swept-wing flows. Research has identified four types of instabilities for these flows: attachment line, streamwise, centrifugal, and crossflow. The attachment-line problem is caused by a basic instability of the attachment-line boundary layer or by its contamination with turbulent disturbances and develops, in general, on swept wings with a large leading-edge radius [24, 25, 44–46]. The streamwise instability is not unlike the familiar Tollmien–Schlichting (TS) wave in two-dimensional flows. This mechanism is associated with the chordwise velocity component and is generally stabilized by a favorable pressure gradient. Centrifugal instabilities can appear over concave regions on the surface and result in the development of Görtler vortices (Floryan [22]; Benmalek and Saric [7]; Saric [59]). Crossflow waves, on the other hand, are an inviscid instability mechanism caused by the combined effect of wing sweep and pressure gradient. All of these instabilities can appear individually or together depending on the combination of Reynolds number, wall curvature, wing sweep, pressure gradient, and external disturbances. Thus, the swept wing provides a rich environment in which to study the stability behavior of three-dimensional boundary layers.

1.1. CROSSFLOW INSTABILITY

The present review focuses on the crossflow instability that occurs on swept wings in regions of strong, favorable pressure gradient. Unlike TS instability, the crossflow problem exhibits stationary ($f = 0$) as well as traveling disturbances that are amplified. Even though both types of waves are present in typical swept-wing flows, transition is usually dominated by either the stationary or the traveling waves. Linear theory predicts that the traveling disturbances are more highly amplified, however many experiments are dominated by stationary waves. Whether the stationary or traveling waves dominate is directly related to the receptivity process. Stationary waves dominate transition in low-disturbance environments, while traveling waves are more important in high-disturbance environments [8–10, 20, 41]. Since the low-disturbance environment is more characteristic of flight, the stationary waves are expected to be more important.

The rotational components of stationary crossflow waves are typically very weak, hence analytical models have long been based on linear theory. However, experiments often show evidence of strong nonlinear effects [12, 13, 18–21, 52, 53]. The resolution of this apparent paradox lies in the understanding of the physical mechanism by which the stationary waves disturb the boundary layer. The key to the stationary disturbance is that the wave fronts are fixed with respect to the model and nearly aligned with the potential-flow direction (i.e., the wavenumber vector is nearly perpendicular to the inviscid streamline). Consequently, although the rotational motion of the wave is weak, its stationary nature produces an *integrated effect* that causes a strong streamwise distortion in the streamwise boundary-layer profile. This integrated effect and the resulting local distortion of the mean boundary layer leads to the modification of the basic state and the early development of nonlinear effects.

An interesting feature of the stationary crossflow waves is the destabilization of secondary instabilities. The streamwise distortions created by the stationary wave are time-independent, resulting in a spanwise modulation of the mean streamwise velocity profile. As the distortions grow, the boundary layer develops an alternating pattern of accelerated, decelerated, and doubly inflected profiles. The inflected profiles are inviscidly unstable, and as such, are subject to a high-frequency secondary instability [33, 37]. This secondary instability is highly amplified and leads to rapid local break down. Because transition develops locally, the transition front is nonuniform in span and characterized by a ‘saw-tooth’ pattern of turbulent wedges.

1.2. LITERATURE SURVEY

There is no shortage of publications in the field of boundary-layer stability and transition; certainly more than can be discussed in detail here. Comprehensive reviews for both two- and three-dimensional flows are given by Arnal [1–4], Mack [36], Poll [45], Saric [58], and Reshotko [55]. Reed *et al.* [50] give an up-to-date discussion of effectiveness and limitations of linear theory in describing boundary-layer instabilities. The reader is referred to these reports for overviews of much of the early work in stability and transition.

Several key papers provide in-depth reviews of stability and transition research in three-dimensional boundary layers and, in particular, swept-wing flows. Much of the early theoretical and experimental work is discussed by Reed and Saric [49]. Swept wings, rotating disks, axisymmetric bodies (rotating cones and spheres), corner flows, and attachment-line instabilities are reviewed, as well as the stability of flows for other three-dimensional geometries. This paper gives an excellent overview of the unique stability problems in three-dimensional flows. For swept wings, a historical account of the early investigations concerning crossflow instability is given, along with a detailed literature survey.

Recently, improvements in both experimental techniques and computational methods have opened the door to a new understanding of transition in three-dimensional boundary layers. This paper will focus on the latest developments, with emphasis on experimental work and relevant comparisons with CFD. In particular, the leading labs for three-dimensional boundary-layer research will be highlighted: Kachanov and co-workers at ITAM, Novosibirsk studying principally traveling crossflow waves; Bippes and co-workers at DLR, Göttingen investigating linear/nonlinear growth and the sensitivity to freestream conditions; Saric and co-workers at Arizona State University (ASU) focusing on the linear/nonlinear growth of stationary crossflow waves and the importance of surface-roughness-induced initial conditions. Both the ITAM and DLR work use a swept flat plate while the ASU model is a simulated infinite-span swept wing.

Bippes (1997) reviews the European contributions to stability and transition in three-dimensional boundary layers and as such is a companion paper to this work. In another paper, Kachanov [31] reviews the efforts in ITAM, Novosibirsk. We therefore concentrate here on the U.S. efforts.

1.3. SUMMARY OF THE LAST SEVEN YEARS

Although crossflow disturbances have been observed experimentally since the early 1950s [23], much of the important advances have occurred within this decade. The primary accomplishments are briefly summarized in the following paragraphs. A more detailed review of recent findings is given in Section 3.

1.3.1. *Micro-Thin Hot-Film Elements*

Multi-element, microthin hot films developed at NASA Langley Research Center have been successfully used at ASU to obtain multi-point measurements in swept-wing flows [18, 38]. The surface-mounted sensors can be distributed in the chordwise direction for multi-point monitoring of the transition location, or with the elements aligned along the stationary crossflow vortex axis for structure identification. The development of these gauges within a controlled transition experiment aided their implementation in the flight environment.

1.3.2. *Secondary Instability*

In early experiments at ASU, Kohama *et al.* [33] show that when the boundary layer is dominated by stationary crossflow instability, transition is caused by high-frequency secondary instability. This instability results from the local distortion of the mean streamwise boundary-layer profile by the stationary disturbance. As the stationary crossflow wave grows downstream, the *mean* boundary layer develops an alternating pattern of accelerated, decelerated, and doubly inflected profiles. Secondary instability develops locally as a result of the inviscidly unstable inflected profiles. The secondary instability is highly amplified, leading to rapid local breakdown and the characteristic ‘saw-tooth’ transition front. Malik *et al.* [37] put the idea on firm footing with an analysis of secondary instability and obtained an agreement with Kohama *et al.* [33].

1.3.3. *Linear Growth*

In the earlier work of Nitschke-Kowsky and Bippes [43], Müller [40], Deyhle *et al.* [21], Kachanov and Tararykin [32], and Kachanov [31], observed that the wavelength and growth rate of the crossflow wave is initially in general agreement with linear theory and is independent of the freestream turbulence level. However, it is reported that superposing a spanwise periodicity on the flow fixes the wavelength of the stationary disturbance.

1.3.4. *Forced Traveling Modes*

Deyhle *et al.* [21] and Kachanov [31] developed techniques to create controlled traveling waves within the boundary layer and observe the growth of traveling modes. The linear theory was verified in this case. The importance of traveling modes and their dependence on freestream conditions and are put into perspective by Bippes [10].

1.3.5. *Sensitivity to Freestream Conditions*

The DLR experiments of Bippes and co-workers provide important results concerning the role of freestream disturbances. Primary findings are reported by Nitschke-Kowsky and Bippes [43], Müller and Bippes [41], Bippes [8, 9], Bippes and Müller [11], Müller *et al.* [42], and Bippes *et al.* [13]. Recent results are summarized by Deyhle *et al.* [21], Lerche and Bippes [34], Deyhle and Bippes [20], and Bippes [10]. These experiments measure both stationary and traveling crossflow waves, however their relative importance in influencing the details of transition is found to depend on the freestream turbulence level. Müller and Bippes [41] describe a series of comparative experiments using the same swept flat plate in both low- and high-turbulence tunnels. Stationary waves are found to dominate transition in the low-disturbance environment, however in the high-turbulence tunnel both growth rate and final amplitude of the stationary disturbance are reduced. At the same time, traveling waves show larger growth rates and dominate transition.

Not only does the type of transition depend on freestream conditions, but Deyhle and Bippes [20] show that transition can be initially delayed by *increasing* the freestream turbulence levels.

In this case, the strong stationary modes are not as effective in causing the secondary instability because of unsteadiness in the boundary layer.

1.3.6. Sensitivity to Roughness

At ONERA-CERT, Arnal *et al.* [6] use isolated roughness to verify the roughness correlation of von Doenhoff and Braslow [61]. This involves using roughness elements as a bypass, that is, transition occurs just downstream of the roughness element.

In the DLR experiments, Müller and Bippes [41] show that stationary waves remain fixed with respect to the model regardless of the wind tunnel in which the experiment is conducted. This indicates that stationary crossflow instability is sensitive to initial conditions provided by surface roughness.

In the work reported by Radeztsky *et al.* [47], the ASU team investigated the sensitivity of stationary crossflow waves to roughness-induced initial conditions by introducing isolated, micron-sized, artificial roughness elements near the leading edge. These experiments show that a single, three-dimensional roughness element can locally amplify the stationary wave leading to premature transition behind the roughness element. Only single roughness elements are used in these tests, and the effects on transition are observed to occur only in the region downstream of the roughness element. Moreover, the roughness element causes early transition only when its diameter is larger than 10% of the most-unstable-mode wavelength and is placed near Branch I of the stationary instability.

1.3.7. Nonlinear Saturation

In all DLR experiments, growth of the stationary and traveling crossflow waves show initial qualitative agreement with the linear theory. However, the disturbance amplitude saturates due to nonlinear effects. Also, the amplitude of the traveling waves shows a spanwise modulation indicating nonlinear interactions with stationary modes.

In experiments at ASU, Reibert *et al.* [52, 53] investigate nonlinear saturation of stationary waves using micron-sized artificial roughness elements to control the initial conditions. Full-span arrays of roughness elements are used to preserve the spanwise periodicity of the disturbance. By forcing the most unstable mode (according to the linear theory), nonlinear saturation of the disturbance amplitude is observed well before transition. Although the initial growth rate increases with increasing roughness height, the saturation *amplitude* remains largely unaffected by changes in the roughness height.

The presence of a large laminar extent of nonlinear saturation gives rise to a certain difficulty in using linear methods – such as e^N or linear PSE – to predict transition. The futility of such approaches is expressed by Arnal [4] and Reed *et al.* [50], who show that linear methods do not work in three-dimensional boundary layers.

1.3.8. Modal Decomposition

Radeztsky *et al.* [48] describe a measurement technique that allows the experimentally obtained stationary crossflow structure to be decomposed into its spatial modes. Using a high-resolution traversing mechanism, hot wires are carefully moved through the boundary layer along a predetermined path. Data are acquired at numerous spanwise locations, from which modal information is extracted using a spatial power spectrum. Reibert *et al.* [53] use a slightly modified technique to move objectively to determine the modal content. Under certain conditions, the amplitude of the fundamental disturbance mode plus eight harmonics are successfully extracted from the experimental data.

1.3.9. *Excitation of Less Unstable Modes*

Using the modal decomposition technique described above, Reibert *et al.* [53] investigate the effect of roughness-induced forcing at a wavelength three times that of the most unstable stationary mode (according to the linear theory). A cascading of energy from the fundamental to high modes (smaller wavelengths) is observed, leading to nonlinear interactions among the fundamental mode and its harmonics. Transition is observed to occur slightly earlier compared to forcing at the most unstable wavelength, and the saw-tooth transition front is much more ‘regular’ in span. These data indicate that nonlinear interactions among multiple modes is important in determining the details of transition.

1.3.10. *Excitation of Subcritical Modes*

Continuing the experiments of Reibert *et al.* [53], Carrillo [14] describes a set of experiments in which stationary crossflow disturbance is forced with Subcritical roughness spacing, that is, the spacing between roughness elements is less than the wavelength of the mode unstable mode. Under these conditions, the rapid growth of the forced mode completely suppresses the linearly most unstable mode, thereby delaying transition beyond its ‘natural’ location (i.e. where transition occurs in the absence of artificial roughness). These data demonstrate that surface roughness can be used to control the stationary crossflow disturbance wavenumber spectrum in order to delay transition on swept wings.

1.3.11. *Structure Identification Using POD*

Using data collected at ASU, Chapman *et al.* [15, 16] apply linear stochastic estimation (LSE) and proper orthogonal decomposition (POD) to identify the spatio-temporal evolution of structures within a swept-wing boundary layer. Detailed measurements are acquired using multi-element hot-film, hot-wire, and cross-wire anemometry. These data allow the POD to objectively determine (based on energy) modes characteristic of the measured flow. Data are acquired through the transition region, from which an *objective* transition-detection method is developed using the streamwise spatial POD solutions.

1.3.12. *CFD Comparisons (DNS)*

Direct numerical simulations (DNS) have historically been constrained by computer resources and algorithmic limitations, however some successes have been achieved in relation to the stationary crossflow problem. Lin [35] performs DNS for stationary waves on an infinite-span swept wing similar to the ASU experiments. Meyer and Kleiser [39] investigate disturbance interactions between stationary and traveling crossflow modes on a swept flat plate using Falkner–Scan–Cooke similarity profiles for the basic state. The results are compared to the experiments of Müller and Bippes [41]. With an appropriate initial disturbance field, the non-linear development of stationary and traveling crossflow modes is simulated reasonably well up to transition. Wintergerste and Kleiser [63] continue this work by using DNS to investigate the breakdown of crossflow vortices in the highly nonlinear final stages of transition.

1.3.13. *CFD Comparisons (PSE)*

Combining the ability to include nonparallel and nonlinear effects with computationally efficient parabolic marching algorithms, the parabolized stability equations (PSE) developed by Herbert [28] have recently been used to successfully model the crossflow instability. For swept-wing flows, nonlinear PSE calculations exhibit the disturbance amplitude saturation characteristic of the DLR and ASU experiments. Wang *et al.* [62] investigate both stationary and traveling

crossflow waves for the swept airfoil used in the ASU experiments and predict nonlinear amplitude saturation for both types of disturbances. It is suggested that the interaction between the stationary and traveling waves is an important aspect of the transition process.

Within the last year, the PSE have been used at ASU to model the growth and development of the stationary crossflow wave with remarkable precision. Using the experimental data of Reibert [51] to guide the initial conditions, Haynes and Reed [27] are able to accurately predict nonlinear amplitude saturation and model the detailed structure and evolution of the stationary crossflow wave. An interesting discovery of Haynes [26] is a hypersensitivity to seemingly negligible streamline and body curvatures in the ASU experiments.

2. Facility and Model

The ASU crossflow experiments are conducted in the Arizona State University Unsteady Wind Tunnel – a low-speed, low-turbulence, closed-circuit facility in which the stability and transition of laminar boundary layers are studied (Saric [57]). The NLF (2)-0415 airfoil model [60] is mounted vertically in the $1.4 \text{ m} \times 1.4 \text{ m} \times 4.9 \text{ m}$ test section. Floor and ceiling contours installed in the test section produce an infinite-span swept-wing flow (Figure 1). With a 45° sweep and a -4° angle of attack, the favorable pressure gradient produces considerable crossflow while suppressing TS modes (Figure 2). The efficacy of the wall liners in establishing spanwise uniform flow is shown in Figure 3 which is a superposition of 100 mean profiles of the streamwise component. The basic-state flow is found to be identical to Reibert *et al.* (1996).

The aluminum surface of the NLF (2)-0415 is hand polished to a $0.25 \text{ }\mu\text{m}$ rms finish in order to establish the smooth base state. Very small roughness elements, of minimum height of $6 \text{ }\mu\text{m}$ ($\text{Re}_k \approx 0.1$), are introduced in a spanwise periodic distribution. These roughness elements linearly excite specific modes within the boundary layer at a level above the background level. Detailed hot-wire measurements within the boundary layer provide two-dimensional maps of the stationary disturbance structure, while spectral techniques are used to identify and follow specific stationary modes. Details of the procedures have been established in [14, 51–53].

3. Nonlinear Interaction and Amplitude Saturation

3.1. NATURAL ROUGHNESS

In the absence of artificial surface roughness, naturally occurring stationary crossflow waves are nonuniform in span due to submicron surface irregularities near the leading edge. This is shown in Figure 4, which displays a contour plot of the normalized boundary-layer velocity at $x/c = 0.55$ for $\text{Re}_c = 2.4 \times 10^6$. The Figure shows that the streamwise velocity u/U_e

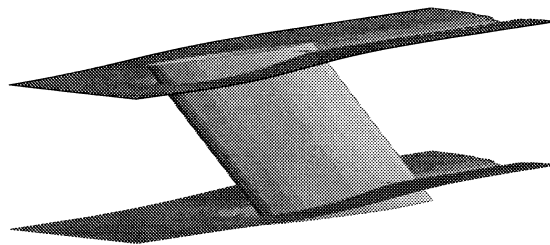


Figure 1. NLF(2)-0415 airfoil and wall liners.

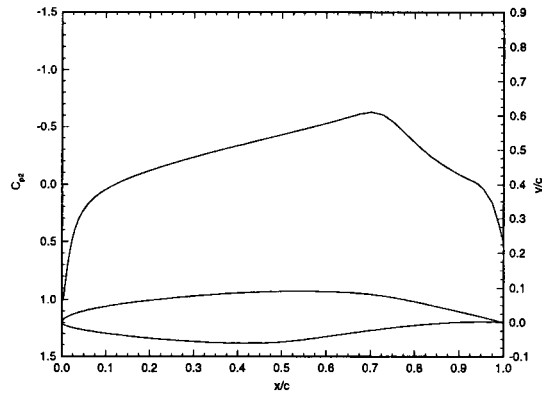


Figure 2. Unswept airfoil and upper surface C_p .

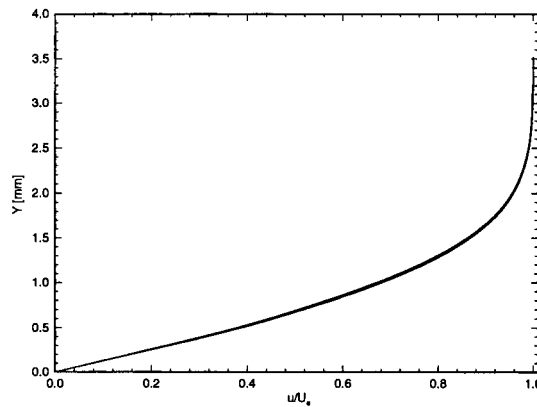


Figure 3. Basic-state boundary layer profiles at $x/c = 0.20$. Plot contains 100 superposed over 99 mm of span.

in the (Y, z) plane. The flow is toward the reader (i.e. the observer is looking upstream into the oncoming boundary-layer flow), and the stationary vortices are turning in the right-handed sense. The velocity contours are constructed from 100 mean-flow boundary-layer profiles each separated by 1 mm in span. It is important to note that the wave-like structure of Figure 4 represents the integrated effect of the weak stationary vortices on the streamwise velocity.

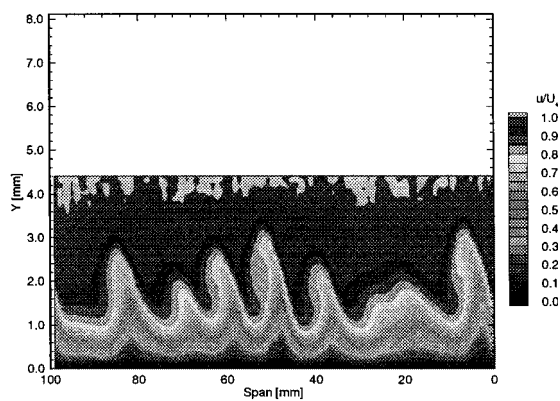


Figure 4. Streamwise velocity contours at $x/c = 0.60$. $Re_c = 2.4 \times 10^6$, no artificial roughness.

Figure 4 displays a dominant feature at a 12 mm spanwise spacing, which is approximately the most amplified stationary wavelength according to the linear theory. At the same time, the richness in the spectral content is evident and indicates nonlinear interaction among many modes. The random nature of the leading-edge roughness leads to the lulls found in the data of Figure 4. These data are typical of all the experiments in the early 1990s. The difficulty with these data is that a computational model will decompose the unstable motion in modes and thus needs the individual mode behavior from the experiment if a meaningful comparison can be made. This information was not forthcoming in the earlier experimental work and Radeztsky *et al.* [48] and Reibert *et al.* [53] corrected the situation by considering a forced response of the boundary layer rather than rely on random disturbances.

3.2. CRITICAL FORCING

Initial conditions are controlled by applying a full-span array of $k = 6 \mu\text{m}$ roughness elements at $x/c = 0.023$. Whereas the height and spanwise spacing may vary, the roughness elements are always placed at the same chord location. At $x/c = 0.023$, displacement thickness is approximately $250 \mu\text{m}$ and $\text{Re}_k \approx 0.1$ for $k = 6 \mu\text{m}$. Thus we expect weak linear input to the unstable waves. The roughness elements are circular and the diameter is 3 mm except in the case of 8 mm spacing in which case the diameter is 2 mm. Radeztsky *et al.* [43] provide data on the effect of chord location and diameter of the roughness.

Spanwise spacing of the elements is 12 mm, corresponding to the naturally occurring most-amplified wavelength. Figure 5 shows the streamwise velocity contour with the roughness installed. The dominance of the 12 mm mode is striking, and allows a direct calculation of the stationary disturbance amplitude (see Reibert *et al.* 1996 for a description of the technique).

Figure 6 compares the experimental amplification factor ('N-factor') for the 12 mm roughness forcing with the predictions of the Orr–Sommerfeld equation (OSE), the linear parabolized stability equations, and the full nonlinear parabolized stability equations. All computational results are provided by Haynes [26]. The saturation phenomenon is clearly evident, and can be quantified. The early growth shows excellent agreement with linear PSE, however strong nonlinear effects develop well before transition at $(x/c)_{tr} = 0.52$. The importance of nonparallel effects is indicated by the failure of traditional linear stability theory (OSE) to accurately predict the growth even in the linear range. When nonlinearity is added, the agreement is remarkable

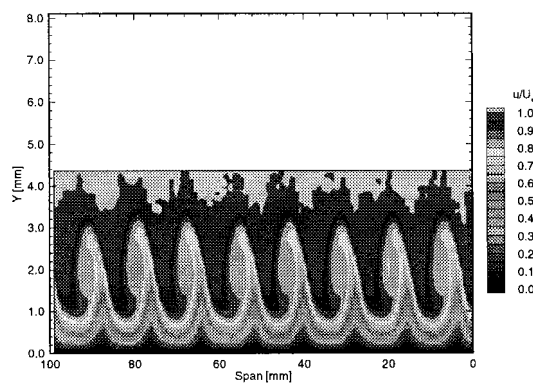


Figure 5. Streamwise velocity contours at $x/c = 0.45$, $\text{Re}_c = 2.4 \times 10^6$, $k = 6 \mu\text{m}$ at 12 mm spacing.

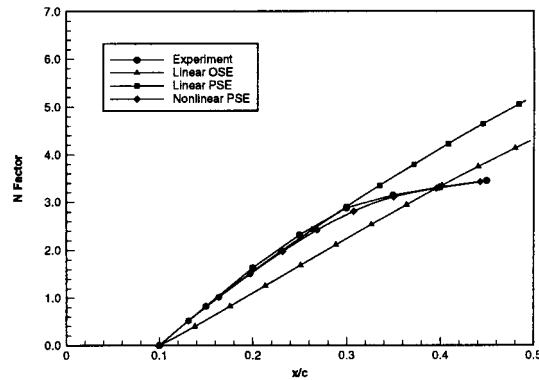


Figure 6. Measured and theoretical N -factors for the conditions of Figure 5. All calculations include curvature (Haynes and Reed [27]).

over the entire measurement region and all aspects of the growth are predicted. This is explained in more detail in [26, 27, 51, 53].

The outstanding agreement shown in Figure 6 results from the inclusion of curvature in the computations, without which the disturbance growth is significantly overpredicted. The sensitivity to very weak curvature is due to the strong stabilizing Görtler effect with convex curvature (Benmalek and Saric [7]). This is the reason for the disagreement between the linear experiments of Radeztsky *et al.* [48] and linear theory without curvature. More information on the sensitivity to curvature can be found in Haynes [26].

3.3. MULTIPLE-MODE CROSSFLOW WAVES

Reibert *et al.* [53] produced multiple-mode crossflow waves by increasing the space between the roughness elements. Their streamwise velocity contours obtained with a roughness spacing of 36 mm showed a primary structure at 36 mm corresponding to the roughness spacing. In addition, higher wavenumber (shorter wavelength) modulations appeared due to superharmonics that are present at integer multiples of the primary wavenumber. This is clearly indicated by the power spectral density (PSD) calculations of Reibert *et al.* [53] which showed amplified modes with wavelengths of 36, 18, 12, 9, 7.2, 6, 5.1, 4.5 and 4 mm. The presence of the roughness-induced harmonic sequence indicates that the stationary crossflow pattern is not predetermined by external flow conditions, but can be completely controlled by the surface characteristics.

4. Role of Spanwise Spacing

Two important observations concerning the data of Reibert *et al.* [53] are

- (1) Unstable waves occur only at integer multiples of the primary disturbance wavenumber, and
- (2) No subharmonic disturbances are destabilized.

In other words, spacing the roughness elements 12 mm apart excites disturbances with spanwise wavelengths of 6 and 4 mm. Spacing the roughness elements 36 mm apart excites disturbances with spanwise wavelengths of 36, 18, 12, 9, 7.1 and 6 mm etc. These spacings do not produce any unstable waves with ‘intermediate’ wavelengths or with wavelengths greater than the imposed spacing.

Table 1. Experimental data sets

Data set	$Re_c/10^6$	Roughness		Scan type	
		$k(\mu\text{m})$	$\lambda_z(\text{mm})$	BL	Span
\mathcal{A}	2.4	0	0	•	•
\mathcal{B}	2.4	6	18	•	•
\mathcal{C}	2.4	12	18	•	•
\mathcal{D}	2.4	18	18	•	•
\mathcal{E}	2.4	6	8	•	•

Following this lead, we investigate the effects of distributed roughness whose primary disturbance wavenumber does not contain a harmonic at $\lambda_s = 12 \text{ mm}$ (the most unstable wavelength according to the linear theory).

4.1. OVERVIEW

All stationary crossflow amplitude data are acquired using the two hot-wire techniques explained in Reibert *et al.* [53]. Table 1 summarizes the five data sets examined in this study. The chord Reynolds number is shown in the column labeled Re_c and is fixed at 2.4×10^6 for all cases. Columns k and λ_z show the roughness height and spanwise spacing, respectively, and the last two columns give the type of scan used. A bullet (•) in the BL and Span columns indicates wall-normal boundary-layer scans and constant- Y spanwise scans, respectively. Note that both scan types are used for all data sets.

To maintain consistency with Reibert [51], the shorthand notation $[k|\lambda_z]$ will be used to unambiguously define the roughness configuration. As outlined in Section 3.2.1, the roughness elements are applied in a full-span array at $x/c = 0.023$ for all cases. Therefore, specifying the roughness height and spacing fully determines the roughness configuration. Thus, $[6|18]$ represents a full-span roughness array with a $k = 6 \mu\text{m}$ element height and a $\lambda_z = 18 \text{ mm}$ spanwise spacing. The natural roughness case, data set \mathcal{A} , is given the notation $[0|0]$.

When presenting the results for individual-mode disturbance amplitudes, crossflow modes will be designated in the shorthand notation (f, m) , where f is the disturbance frequency and m is the mode number. The mode number is defined as the disturbance wavenumber normalized by the wavenumber of the fundamental mode. Thus, $m = 1$ and $m = 2$ indicate the fundamental disturbance and first superharmonic, respectively. The spanwise-invariant disturbance, typically called the ‘mean-flow distortion’ mode, is presented by $(0,0)$.

4.2. NATURAL ROUGHNESS - DATA SET \mathcal{A}

Some of these data have been presented in Figures 3 and 4 while the remainder are referenced to Carrillo [14]. Extensive measurements were carried out in this case to archive the natural roughness base state should anyone wish to tackle a computation of these results. Information on flow visualization and transition location will be discussed in a later section.

4.3. [6 | 18] ROUGHNESS – DATA SET \mathcal{B}

To generate stationary crossflow waves that are uniform in span and contain a fixed spectral content, artificial surface roughness elements are applied to the airfoil surface as explained in Section 3.2.1. These roughness elements provide fixed initial conditions for the stationary vortices. A full-span array of $6\ \mu\text{m}$ high roughness elements spaced 18 mm apart is applied at $x/c = 0.023$. Radeztsky *et al.* [47] shows that this chord location maximizes the effects of the applied roughness.

The 18 m spacing was chosen to confirm that neither the 12 mm mode nor the 36 mm mode will be excited according to the observations described at the beginning of Section 4.

4.3.1. Total Disturbance Amplitude

Figure 7 shows the normalized velocity contours at $\text{Re}_c = 2.4 \times 10^6$ at $x/c = 0.40$. The 18 mm spacing is observed with a very strong 9 mm modulation. Even at $x/c = 0.45$, the small artificial roughness yields boundary-layer distortions that are very uniform and periodic in span.

Boundary-layer profiles from which the contour map of Figure 7 is made are shown in Figure 8. The mean profile is also shown and as with the no roughness case, the stationary disturbance has dramatically distorted the mean boundary layer. The spanwise-average profile is doubly inflected even for $x/c \geq 0.30$.

Figure 9 presents the total disturbance mode-shape profiles for $0.10 \leq x/c \leq 0.45$. Following [53], departure from the linear mode shapes begin to occur around $x/c = 0.3$. The growth of the disturbance is easily characterized by the log of the amplitude ratio such as $N = \ln(A/A_0)$. Where A_0 is the initial amplitude and N is commonly called the N -factor. The *measure* of the disturbance can be (1) the maximum of the rms mode shape; (2) the integral of the rms in the wall-normal direction; (3) the integral of the square of the rms. Reibert *et al.* [53] show that when cast in terms of the N -factor, the growth behavior is the same. Thus the max amplitude of the mode shapes of Figure 9 are used as a measure of growth. The top curve of Figure 10 is the growth of total signal. This curve shows dramatic amplitude saturation for $x/c \geq 0.25$. At these chord locations, the characteristic second lobe appears in the mode-shape profiles, indicating strong nonlinear effects.

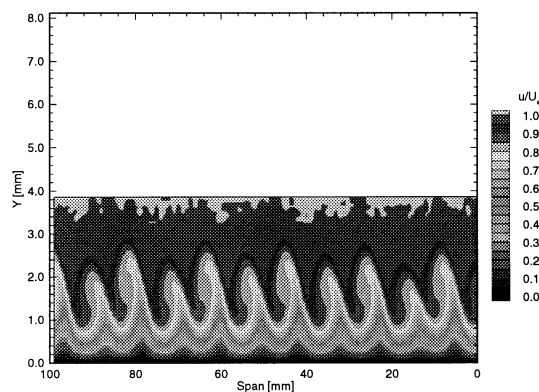


Figure 7. Streamwise velocity contours at $x/c = 0.40$. $\text{Re}_c = 2.4 \times 10^6$. $k = 6\ \mu\text{m}$ at 18 mm spacing.

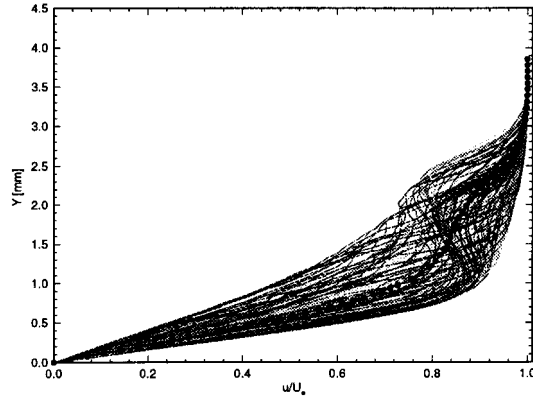


Figure 8. Spanwise array of 100 profiles spaced 1 mm apart at $x/c = 0.40$. $Re_c = 2.4 \times 10^6$. $k = 6 \mu\text{m}$ at 18 mm spacing.

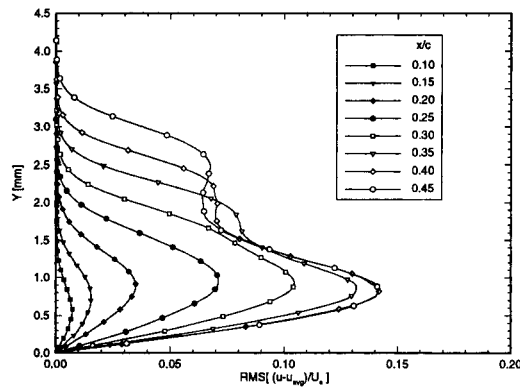


Figure 9. Stationary crossflow mode shapes. Conditions of Figure 8.

4.3.2. Individual-Mode Amplitude

A full set of spanwise scans are conducted to extract the modal content of the disturbance. The height scanned corresponds to the maximum of the total disturbance mode shape at each x/c . The power spectral density computations for these scans are computed. Integration of the peaks of these data are used to form Figure 10. Unstable modes are first detected at $x/c = 0.10$. The

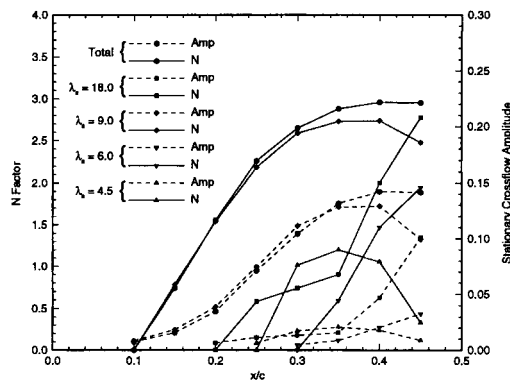


Figure 10. Total and single-mode disturbance amplitudes and N -factors. Conditions of Figure 8.

spectrum at this location shows energy in the (0,2) mode ($\lambda_z = 9$ mm). Although there is a peak evident at λ_z mm, its amplitude is very small and close to the noise of the spectrum. Based on a consistent definition of the spectral noise, the 18 mm peak is ignored. It is interesting that the (0,2) mode contains more energy than the fundamental ($\lambda_z = 18$ mm).

The fundamental mode is not measurable until $x/c = 0.20$. Although the fundamental is detected, the first harmonic at $\lambda_z = 9$ mm still contains most of the disturbance energy. The fundamental disturbance grows rapidly for $0.35 \leq x/c \leq c \leq 0.45$, where the (0,2) mode actually shows some decay. Higher harmonics become unstable for $x/c \geq 0.25$. The spectrum at $x/c = 0.45$ shows detectable disturbances for the (0,3) and (0,4) modes ($\lambda_z = 6$ and 4.5 mm). No amplified subharmonics (wavelength doubling) of the roughness spacing are detected. This is consistent with the findings of [53].

Note that the 12 mm wavelength, which is approximately the most unstable according to the linear theory, is not amplified at any x/c . The 18 mm forcing has successfully suppressed the growth of this wavelength disturbance. Reibert *et al.* [53] did not observe this because his roughness spacings were all multiples of 12 mm. Radeztsky *et al.* [48] does show this phenomenon, however, his studies were at a different angle of attack ($\alpha = 0^\circ$) with much larger roughness heights (146 μm).

In Figure 10 the (0,2) mode shows exponential growth up to $x/c = 0.25$, at which point the mode begins to saturate. The (0,2) mode reaches a maximum amplitude of 13% at $x/c = 0.40$, after which it decays. It is in this saturation and decay region ($0.35 \leq x/c \leq 0.45$) of the (0,2) mode where the fundamental disturbance shows strong growth. This is also the region of strong nonlinear effects as seen by the growth of the second lobe in the total disturbance mode-shape profiles (Figure 9).

Also presented in Figure 10 are the corresponding N -factor distributions. Since the individual modes are first detected at different chord locations with different initial amplitudes, each wavelength N -factor curve is reference to a different amplitude. Thus, direct comparisons between the growth *rates*, however, are entirely meaningful. The amplitude of the (0,2) mode ($\lambda_z = 9$ mm) agrees well with the total disturbance amplitude up to $x/c = 0.30$, the (0,2) mode amplitude drops from the total disturbance and the amplitudes of the fundamental and higher harmonics grow.

The most important feature of Figure 10, however, is that *the linearly most unstable disturbance* ($\lambda_s = 12$ mm) *has been completely suppressed*.

4.4. [12 | 18] AND [18 | 18] ROUGHNESS - DATA SETS \mathcal{C} AND \mathcal{D}

Reibert (1996) observed the interesting feature that, for a fixed roughness spacing of $\lambda_z = 12$ mm, the total disturbance amplitude grew to a constant saturation amplitude even when the roughness height was varied from 6 to 48 μm . Although the initial disturbance amplitude increased with larger roughness, the effects downstream relaxed and yielded similar looking mode shape. Data Sets \mathcal{C} and \mathcal{D} provide further evidence of this characteristic for the $\lambda_z = 18$ mm roughness spacing.

The roughness height in this study is increased from 6 to 12 μm and then to 18 μm by stacking the roughness elements. Transition occurs at $x/c \approx 0.50$ for all three roughness heights. Since saturation amplitude comparisons are the primary concern, disturbance amplitude data are acquired only at $x/c = 0.45$. Both the total disturbance and individual-mode disturbance amplitudes are computed and compared. The details are given in Carrillo (1996).

Table 2. Total and individual-mode amplitudes for $Re_c = 2.4 \times 10^6$ and $[k | 18]$ roughness at $x/c = 0.45$

Roughness Height (μm)	Disturbance mode amplitude (%)				
	Total	$\lambda_z = 18 \text{ mm}$	$\lambda_z = 9 \text{ mm}$	$\lambda_z = 6 \text{ mm}$	$\lambda_z = 4.5 \text{ mm}$
6	14.2	10.1	10.0	3.3	0.9
12	14.8	12.8	8.3	2.7	0.5
18	13.3	11.2	8.0	0.8	0.9

Table 2 summarizes the amplitudes for the total and individual-mode disturbances at $x/c = 0.45$. As mentioned in the previous section, the total disturbance amplitude remains constant at about 14% with increasing roughness height. There does appear to be some redistribution of energy in the modal content as the initial conditions are increased. It is difficult, however, to make any meaningful conclusions about the effects of the larger roughness on the individual-mode amplitudes. As shown by the $[6 | 18]$ roughness, forcing at $\lambda_z = 18 \text{ mm}$ actually excites the 9 mm wavelength first, which grows rapidly, saturates, and then *decays*. It is possible that the larger roughness heights yield larger initial amplitudes for the 9 mm component, which would then grow, saturate, and decay sooner than for the $[6 | 18]$ roughness case. This would explain the smaller (0,2) mode amplitudes, since the mode would be decaying over a larger distance by the time $x/c = 0.45$ is reached. Of course this is all just speculation, and further study must be done before any definite conclusions can be made.

4.5. $[6 | 18]$ ROUGHNESS - DATA SET \mathcal{E}

Section 4.4 shows the effective suppression of the most unstable wavelength by using a roughness spacing that does not contain superharmonics with wavelengths around 12 mm. In addition, no evidence of subharmonics in this and past experiments by Radeztsky *et al.* [48] or Reibert *et al.* [53] has ever been observed. Linear stability theory predicts that short wavelength disturbances grow early, saturate, and then decay. Thus, the next logical step is to study the effects of a subcritical roughness spacing ($\lambda_z < 12 \text{ mm}$).

Both the linear stability theory and the 18 mm-spaced roughness experiments presented above show that the 9 mm wavelength is also very unstable. Therefore, it is desirable to space the roughness elements less than 9 mm apart. For this study, the 6 μm -high roughness elements are applied in a full-span array at $x/c = 0.023$ with a spanwise spacing of 8 mm.

Normalized velocity contours for $Re_c = 2.4 \times 10^6$ and $[6 | 18]$ roughness are shown in Figures 11 and 12 for chord locations $x/c = 0.30$ and 0.60 , respectively. The disturbance is first measurable at $x/c = 0.10$, and a very uniform and dominant $\lambda_z = 8 \text{ mm}$ mode develops for $0.10 \leq x/c \leq 0.25$. At $x/c = 0.30$ (Figure 11), although the contour plot still shows a dominant 8 mm mode, there is noticeable development of some slight nonuniformity. This nonuniformity becomes more dramatic with increasing x/c , and the 8 mm structure fades out in favor of some longer wavelength disturbances. By $x/c = 0.50$, the dominance of the fundamental mode ($\lambda_z = 8 \text{ mm}$) is gone, and $x/c = 0.60$ (Figure 12) the fundamental mode is indistinguishable in the velocity contours.

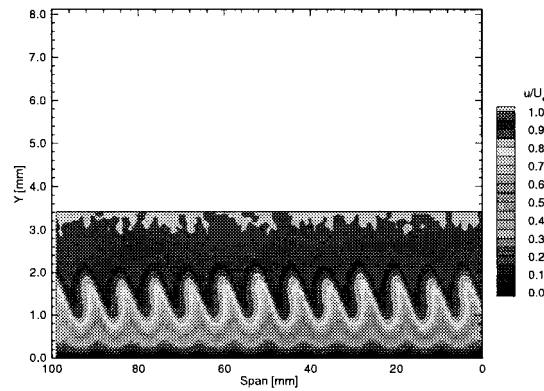


Figure 11. Streamwise velocity contours at $x/c = 0.30$. $Re_c = 2.4 \times 10^6$. $k = 6 \mu\text{m}$ at 8 mm spacing.

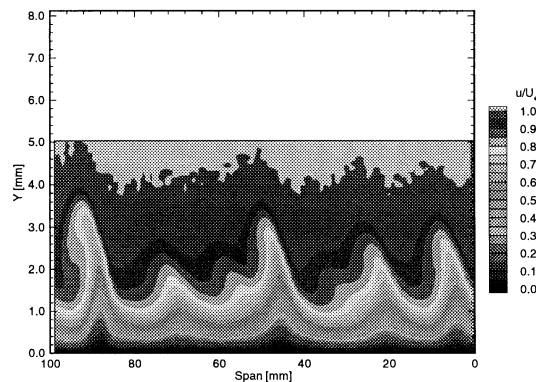


Figure 12. Streamwise velocity contours at $x/c = 0.60$. Conditions of Figure 11.

The total disturbance amplitude N -factors computed from the mode shapes show that the total disturbance grows rapidly from $0.10 \leq x/c \leq 0.30$, at which point the amplitude saturates and then shows strong decay. At $x/c = 0.30$, the second lobe high in the mode shape is evident, indicating strong nonlinear effects. The amplitude continues to decay for $0.30 \leq x/c \leq 0.45$. At $x/c = 0.45$, the amplitude levels off and then shows a second region of strong growth for $0.50 \leq x/c \leq 0.60$.

In short, $Re_c = 2.4 \times 10^6$ and [6 | 18] roughness delays transition past that of the natural roughness case. Strong early growth of the 8 mm mode effectively suppresses initial growth of the very unstable 9 mm and 12 mm modes near the leading edge, which the linear stability theory predicts to be the region where these modes have the largest growth rates. The fundamental ($\lambda_z = 8$ mm) mode saturates and then decays rapidly. This dramatic decay allows for longer wavelength background disturbances (due to submicron surface irregularities) to become unstable. The growth of these longer-wavelength broadband disturbances eventually leads to transition.

5. Conclusions

Boundary-layer transition in three-dimensional flows is a complicated process involving complex geometries, multiple instability mechanisms, and nonlinear interactions. Yet significant progress has been recently made toward understanding the stability and transition characteristics

of swept-wing flows. Concerning the crossflow problem, the past seven years have produced several important discoveries including

- development of instrumentation that can be applied to the flight-test environment,
- application of POD methods to interpret wind-tunnel and flight-test transition data,
- effect of environmental conditions in determining the relative importance of stationary and traveling waves,
- existence of a secondary instability causing local transition in stationary-crossflow-dominated flows,
- sensitivity of the stationary disturbance to leading-edge surface roughness,
- importance of nonlinear effects and modal interaction,
- development of nonlinear PSE codes to predict all aspects of stationary disturbance growth,
- sensitivity of stationary wave growth to very weak convex curvature,
- use of artificial roughness to control the disturbance wavenumber spectrum and delay transition.

Three-dimensional boundary-layer stability is still far from being completely explained. Important factors such as receptivity – the process by which external disturbances enter the boundary layer and create the initial conditions for an instability – are still not well understood. Yet in spite of these shortcomings, careful experiments and accurate computations have resulted in significant progress toward understanding a difficult problem.

Acknowledgements

This work was supported by NASA Langley Research Center Cooperative Agreement NCC-1-194 and Boeing Contract ZA0078. The authors thank Dr. Keith Chapman for his contributions – both past and present – to the ASU Unsteady Wind Tunnel. The numerical calculations of Drs. Tim Haynes and Helen Reed are gratefully acknowledged. The technical support of Mr. Dan Clevenger is greatly appreciated.

References

1. Arnal, D., 'Description and prediction of transition in two-dimensional incompressible flow', In: *Special Course on Stability and Transition of Laminar Flows*, AGARD R-709, 1984, pp.-1–2-71.
2. Arnal, D., 'Three-dimensional boundary layers: Laminar-turbulent transition', In: *Special Course on Calculation of Three-Dimensional Boundary Layers with Separation*, AGARD R-741, 1986, pp. 1-1–1-34.
3. Arnal, D., 'Boundary-layer transition: Prediction, application to drag reduction', In: *Special Course on Skin Friction Drag Reduction*, AGARD R-786, Loughton, Essex, 1992, pp. 5-1–5-59.
4. Arnal, D., 'Boundary-layer transition: Predictions based on linear theory', In: *Special Course on Progress in Transition Modelling*, AGARD R-793, Loughton, Essex, 1994, pp. 2-1–2-63.
5. Arnal, D., *Laminar-Turbulent Transition: Research and Applications in France*, AIAA Paper 97-1905.
6. Arnal, D., Casalis, G. and Juillen J.C., 'Experimental and theoretical analysis of natural transition on infinite swept wing', In: D. Arnal and R. Michel (eds), *Laminar-Turbulent Transition*, vol. 3, Springer-Verlag, Berlin, pp. 311–325.
7. Benmalek, A. and Saric, W.S., 'Effects of curvature variations on the nonlinear evolution of Goertler vortices', *Phys. Fluids* 3(10) (1994) 3353–3367.
8. Bippes, H., 'Instability feature appearing on swept wing configurations', In: D. Arnal and R. Michel (eds), *Laminar-Turbulent Transition*, vol. 3, Springer-Verlag, Berlin, 1990, pp. 419–430.
9. Bippes, H., 'Experiments on transition in three-dimensional accelerated boundary-layer flows', In: *Proc. R.A.S. Boundary Layer Transition and Control*, Cambridge, U.K., 1991.

10. Bippes, H., *Environmental Conditions and Transition Prediction in 3-D Boundary layers*, AIAA Paper **97-1906**, 1997.
11. Bippes, H. and Müller, B., 'Disturbance growth in an unstable three-dimensional boundary layer,' In: T. Cebeci (ed.), *Numerical and Physical Aspects of Aerodynamics Flows IV*, Springer-Verlag, Berlin, 1990, pp. 345–358.
12. Bippes, H. and Nitschke-Kowsky, P., 'Experimental study of instability modes in a three-dimensional boundary layer', *AIAA J.* **28**(10) (1990) 1758–1763.
13. Bippes, H., Müller, B. and Wagner, M., 'Measurements and stability calculations of the disturbance growth in an unstable three-dimensional boundary layer', *Phys. Fluids* **3**(10) (1991) 2371–2377.
14. Carrillo, R.B. Jr., *Distributed-Roughness Effects on Stability and Transition in Swept-Wing Boundary Layers*. Master's thesis, Arizona State University, 1996.
15. Chapman, K.L., Glauser, M.N., Reibert, M.S. and Saric, W.S., 'Proper orthogonal decomposition applied to boundary-layer transition on a swept wing', In: R.A.W.M. Henkes and J.L. van Ingen (eds), *Transitional Boundary Layers in Aeronautics*, Amsterdam, North-Holland Press, 1995, pp. 165–173.
16. Chapman, K.L., Glauser, M.N., Reibert, M.S. and Saric, W.S., 'A Multi-Point Correlation Analysis of a Crossflow-Dominated Boundary Layer', AIAA Paper **96-0186**, 1996.
17. Crouch, J., *Transition Prediction and Control for Airplane Applications*, AIAA Paper **97-1907**, 1997.
18. Dagenhart, J.R., Saric, W.S., Mousseux, M.C., Stack, J.P., *Crossflow Vortex Instability and Transition on a 45-Degree Swept Wing*, AIAA Paper **89-1892**, 1989.
19. Dagenhart, J.R., Saric, W.S., Hoos, J.A. and Mousseux, M.C., 'Experiments on swept-wing boundary layers', In: D. Arnal and R. Michel (eds), *Laminar-Turbulent Transition*, vol. 3, Springer-Verlag, Berlin, 1990, pp. 369–380.
20. Deyhle, H. and Bippes, J., 'Disturbance growth in an unstable three-dimensional boundary layer and its dependence on environmental conditions', *J. Fluid Mech.* **316** (1996) 73–113.
21. Deyhle, H., Höhler, and Bippes, H., 'Experimental investigation of instability wave propagation in a 3-D boundary-layer flow', *AIAA J.* **31**(4) (1993) 637–645.
22. Floryan, J.B., 'On the Görtler instability of boundary layers', *Prog. Aerospace Sci.* **28** (1991) 235–271.
23. Gray, W.E., 'The effect of wing swept on laminar flow', RAE TM Aero **255**, 1952.
24. Hall, P. and Malik, M.R., 'On the instability of a three-dimensional attachment-line boundary layer: Weakly nonlinear theory and a numerical approach', *J. Fluid Mech.* **163** (1986) 257–282.
25. Hall, P., Malik, M.R. and Poll, D.I.A., 'On the stability of an infinite swept attachment-line boundary layer', *Phil. Trans. Roy. Soc. Lon. A* **395** (1984) 229–245.
26. Haynes, T.S., *Nonlinear Stability and Saturation of Crossflow Vortices in Swept-Wing Boundary Layer*, PhD dissertation, Arizona State University, 1996.
27. Haynes, T.S. and Reed, H.L., *Computations in Nonlinear Saturation of Stationary Crossflow Vortices in a Swept-Wing Boundary Layer*, AIAA Paper **96-0182**, 1996.
28. Herbert, T., 'Parabolized stability equations', In: *Special Course on Progress in Transition Modelling*, AGARD R-793, Loughton, Essex, 1994, pp. 4-1–4-34.
29. Herbert, T., *Transition Analysis of Flow over Aerodynamic Bodies*, AIAA Paper **97-1908**, 1997a.
30. Herbert, T., *On the Stability of 3-D Boundary Layers*, AIAA Paper **97-1961**, 1997b.
31. Kachanov, Y.S., *Experimental Studies of Three-Dimensional Instability of Boundary Layer*, AIAA Paper **96-1976**, 1996.
32. Kachanov, U.S. and Tararykin, O.I., 'The experimental investigation of stability and receptivity of a swept-wing flow', In: D. Arnal and R. Michel (eds), *Laminar-Turbulent Transition*, vol. 3, Springer-Verlag, Berlin, 1990, pp. 499–509.
33. Kohama, Y., Saric, W.S. and Hoos, J.A., 'A high-frequency secondary instability of crossflow vortices that leads to transition', In: *Proc. R.A.S. Boundary Layer Transition and Control*, Cambridge, U.L., 1991.
34. Lerche, T. and Bippes, H., 'Experimental investigation of cross-flow instability under the influence of controlled disturbance excitation', In: R.A.W.M. Henkes and J.L. van Ingen (eds), *Transitional Boundary Layers in Aeronautics*, Amsterdam, North-Holland Press, 1995, pp.137–144.
35. Lin, R.-S., *Stationary Crossflow Instability on Infinite Swept Wing*, PhD Dissertation, Arizona State University, 1992.
36. Mack, L.M., 'Boundary-layer linear stability theory', In: *Special Course on Stability and Transition of Laminar Flows*, AGARD R-709, 1984, pp. 3-1–3-81.
37. Malik, M.R., Li, F. and Chang, C.L., 'Crossflow disturbances in three-dimensional boundary layers: Nonlinear development, wave interaction and secondary instability', *J. Fluid Mech.* **268** (1994) 1–36.

38. Mangalam, S.M., Maddalon, D.V., Saric, W.S. and Agarwal, N.K., *Measurement of Crossflow Vortices, Attachment-Line Flow, and Transition Using Microthin Hot Films*, AIAA Paper **90-1636**, 1990.
39. Meyer, F. and Kleiser, L., 'Numerical simulation of transition due to crossflow instability', In: D. Arnal and R. Michel (eds.), *Laminar-Turbulent Transition*, vol. 3, Springer-Verlag, Berlin, 1990, pp. 609–619.
40. Müller, B., 'Experimental study of travelling waves in a three-dimensional boundary layer', In: D. Arnal and R. Michel (eds.), *Laminar-Turbulent Transition*, vol. 3, Springer-Verlag, Berlin, 1990, pp. 489–498.
41. Müller, B. and Bippes, H., 'Experimental study of instability modes in a three-dimensional boundary layer', In: *Fluid Dynamics of Three-Dimensional Turbulent Shear Flows and Transition*, AGARD CP-438, Loughton, Essex, 1989, pp. 13-1–13-15.
42. Müller, B., Bippes, H. and Collier, F.S. Jr., 'The stability of a three-dimensional boundary layer over a swept flat plate', In: M.Y. Hussaini and R.G. Voight (eds), *Instability and Transition*, vol. 2, Springer-Verlag, New York, 1990, pp. 268–277.
43. Nitschke-Kowsky, P. and Bippes, H., 'Instability and Transition of a three-dimensional boundary layer on a swept flat plate', *Phys. Fluids* **31**(4) (1988) 786–795.
44. Poll, D.I.A., 'Transition in the infinite swept attachment line boundary layer', *Aeronaut. Q.* **30** (1979) 607–629.
45. Poll, D.I.A., 'Transition description and prediction in three-dimensional flows', In: *Special Course on Stability and Transition of Laminar Flows*, AGARD R-709, 1984, pp. 5-1–5-23.
46. Poll, D.I.A., 'Some observations of the transition process on the windward face of a long yawed cylinder,' *J. Fluid Mech.* **150** (1985) 329–356.
47. Radeztsky, R.H. Jr., Reibert, M.S., Saric, W.S. and Takagi, S., *Effect of Micron-Sized Roughness on Transition in Swept-Wing Flows*, AIAA Paper **93-0076**, 1993.
48. Radeztsky, R.H. Jr., Reibert, M.S. and Saric, W., *Development of Stationary Crossflow Vortices on a Swept Wing*, AIAA Paper **94-2373**, 1994.
49. Reed, H.L. and Saric, W.S., 'Stability of three-dimensional boundary layers', *Ann. Rev. Fluid Mech.* **21** (1989) 235–284.
50. Reed, H.L., Saric, W.S. and Arnal, D., 'Linear stability theory applied to boundary layers', *Ann. Rev. Fluid Mech.* **28** (1996) 389–428.
51. Reibert, M.S., *Nonlinear Stability, Saturation, and Transition in Crossflow-Dominated Boundary Layers*, PhD Dissertation, Arizona State University, 1996.
52. Reibert, M.S., Saric, W.S., Carrillo, R.B., Jr. and Chapman, K.L., 'Nonlinear stability, saturation, and transition in swept-wing flows', In: R.A.W.M. Henkes and J.L. van Ingen (eds), *Transitional Boundary Layers in Aeronautics*, Amsterdam, North-Holland Press, 1995, pp. 125–135.
53. Reibert, M.S., Saric, W.S., Carrillo, R.B., Jr. and Chapman, K.L., *Experiments in Nonlinear Saturation of Stationary Crossflow Vortices in a Swept-Wing Boundary Layer*, AIAA Paper **96-0184**, 1996.
54. Reibert, M.S. and Saric, W.S., *Review of Swept-Wing Transition*, AIAA Paper **97-1816**, 1997.
55. Reshotko, E., *Boundary Layer Instability, Transition and Control*, AIAA Paper **92-3910**, 1994.
56. Reshotko, E., *Progress, Accomplishments and Issues in Transition Research*, AIAA Paper **97-1815**, 1997.
57. Saric, W.S., *The ASU transition research facility*, AIAA Paper **92-3910**, 1992a.
58. Saric, W.S., 'Laminar-turbulent transition: Fundamentals', In: *Special Course on Skin Friction Drag Reduction*, AGARD R-786, 1992b, pp. 4-1–4-32.
59. Saric, W.S., 'Görtler vortices', *Ann. Rev. Fluid Mech.* **26** (1994) 379–409.
60. Somers, D.M. and Horstmann, K.H., 'Design of a medium-speed natural-laminar-flow airfoil for commuter aircraft applications', *DFVLR-IB/29-85/26*, 1985.
61. von Doenhoff, A.E. and Braslow, A.L., 'The effect of distributed roughness on laminar flow', In: Lachmann, (ed), *Boundary-Layer Control*, vol. 2, Pergamon, 1961.
62. Wang, M., Herbert, T. and Stuckert, G.K., *Crossflow-Induced Transition in Compressible Swept-Wing Flows*, AIAA Paper **94-2374**, 1994.
63. Wintergerste, T. and Kleiser, L., 'Direct Numerical Simulation of transition in a three-dimensional boundary layer', In: R.A.W.M. Henkes and J.L. van Ingen (eds), *Transitional Boundary Layers in Aeronautics*, Amsterdam, North-Holland Press, 1995, pp. 145–154.